Available online at www.sciencedirect.com

ScienceDirect

Energy Procedia 53 (2014) 184 – 192

Energy Procedia

EERA DeepWind'2014, 11th Deep Sea Offshore Wind R&D Conference

Sea Surface Gravity Wave-Wind Interaction in the Marine Atmospheric Boundary Layer

M. Bakhoday Paskyabi[a,*], S. Zieger[b], A.D. Jenkins[c], A.V. Babanin[b], D. Chalikov[b]

[a] *Geophysical Institute, University of Bergen, Bergen, Norway*
[b] *Centre for Ocean Engineering, Science and Technology Swinburne University of Technology Melbourne, Australia*
[c] *Uni Research Computing, Bergen, Norway*

Abstract

In this study, we investigate the turbulence structure over idealized wind-generated surface gravity waves with varying wave age using a wave-modified one-dimensional boundary layer model. To prescribe the shape of the water wave and the associated orbital velocities, we employ an empirical expression for the wave energy spectrum without assigning a prognostic equation for modelling wave evolution under the action of wind. The key element in this model is the the work done by the wave-induced momentum flux on the atmosphere in the presence of waves. This is incorporated into the airflow using an exponential decay function. Finally, we conduct a series of numerical experiments to identify wave effects on the airflow over a wavy moving interface as a function of wave age, and to check the skill of the present model in capturing wave-induced processes in the marine atmospheric boundary layer (MABL). The results obtained confirm again the significant role of wave-induced processes in influencing the MABL, for example, in modifying the wind profile. Meanwhile, it is shown that the modified one-dimensional model is sensitive to wave parameterizations and the wave energy spectrum. However, a number of uncertainties remain for further investigation, such as the choice of wave energy spectrum, wave forcing parametrization, and surface boundary conditions for momentum and energy.

Selection and peer-review under responsibility of SINTEF Energi AS
Keywords: Swell; Wave-induced wind; Wave-current interactions;

1. Introduction

Ocean surface gravity waves, as a ubiquitous phenomenon in the world ocean, set a restless boundary between the atmosphere and the ocean. Due to the role of surface gravity waves for various air-sea interaction processes, they are important features of the air-sea interaction for both ocean engineers and atmospheric and ocean scientists [1]. All marine structures and installations in deep and shallow coastal ocean regions require wave climate information as a substantial input for design, installation, and maintenance. In addition to industrial requirements for the understanding of wave forcing effects, wave processes have attracted great attention from oceanographers and meteorologists due to their significant role in the exchange of momentum, heat, energy, gas, and moisture across the air-sea boundary.

* M. Bakhoday Paskyabi.
E-mail address: Mostafa.Bakhoday@gfi.uib.no

Selection and peer-review under responsibility of SINTEF Energi AS
doi:10.1016/j.egypro.2014.07.227

Moreover, a better knowledge of these exchange mechanisms at the air-sea interface is beneficial for climate and ocean modelling and the prediction of ocean waves and storm surges.

Swell (waves which have propagated away from their generation area) comprise part of the wave energy spectrum which may be responsible for the upward transfer of momentum and energy from the ocean to the atmosphere. To date, the idea of wave-induced momentum and energy injection into the MABL close to the wavy interface was reported first by Harris [2], and has been confirmed by subsequent field observations and laboratory experiments. Fabrikant [3] and Janssen [4] analysed wave-wind interaction by developing a quasi-linear interaction mechanism which applied Miles' [5] wave generation theory. Jenkins [6] applied the Miles and Fabrikant quasi-linear theory together with a simplified form of the wind velocity profile to show that the 10 m drag coefficient increases with wave age at small wave ages, and decreases again at large wave ages. Jenkins [7] employed quasi-linear wave generation and an eddy viscosity turbulence closure scheme in surface following coordinates to compute wave generation and air-sea momentum flux due to wave–mean flow interaction in the entire MABL (in addition to the interaction at the critical level where the wave phase velocity is equal to the wind velocity, which determines the rate of wave generation in the Miles [5]) theory. Sullivan et al. [8] studied the turbulence structure over a wavy wall using Direct Numerical Simulation (DNS) and Large Eddy Simulation (LES) techniques. Their result suggested that in-line wind and swell results in a low-level jet as a responsible mechanism for transferring of energy from waves to the overlying wind. Kudryavtsev et al. [9] studied the interactions between swell and the MABL based on a two-layer approximation for the boundary layer. They showed that the wave age characterizes the swell impact on the MABL with stronger impacts for steeper swells. Belcher and Hunt [10] reviewed theoretical studies on turbulent flow over wavy terrain with no discussion of swell effects. Semedo [11] highlighted that moving swells affect the overlying wind by imposing acceleration of the flow in the lower surface MABL, resulting in the formation of a low-level wind jet. In addition to the aforementioned effects, waves can also affect the aerodynamic characteristics of the airflow through formation of flow separation regions and alteration of the surface roughness length.

Yelland and Taylor [12] reported an increase of the drag coefficient, C_D, under low wind speeds in the open ocean. Donelan et al. [13] found that the drag coefficient increases at low wind speed when swell propagates across or opposite to the wind. Thus swells directly influence the surface roughness and attenuate the wind seas. Babanin and Makin [14] suggested that C_D depends on the directional spreading of the surface waves along with other possible factors. Chalikov and Rainchik [15] (hereafter CR11) studied numerically the dependence of C_D on wind speeds and directional spreading of the wave field. Ting et al. [16] used the CR11 derived one-dimensional model to study the interaction between C_D and wave field.

To simplify the computation of wave and atmosphere interactions, we use a one-dimensional k–ε turbulence mixing model for the MABL based on CR11 configurations. We present the derivation of this wave-modified model which includes wave effects in both the momentum and energy equations. Due to the complexity of wind-wave interactions, in this paper we only study the vertical distribution of the dissipation rate of Turbulent kinetic Energy (TKE) within the MABL, for varying wave ages and wind speeds.

2. Theoretical background

Traditional equations of motion and energy equations within the MABL, over the sea surface, disregard the effects of wave forcing in the exchange of momentum, energy, and tracers at the air-sea interface. However, the foregoing review of observational and theoretical studies suggests that surface gravity waves have substantial effects on the various physical processes across the air-sea boundary. To account for wave effects on the momentum and energy equations, a milestone stage would be the decomposition of velocity and pressure fields into mean, wave, and turbulence components as follows:

$$\mathbf{u} = \bar{\mathbf{u}} + \tilde{\mathbf{u}} + \mathbf{u}', \quad \text{and} \quad p = \bar{p} + \tilde{p} + p' \tag{1}$$

where bars, tildes, and primes denote time-averaging over scales which remove waves and turbulence contributions, time-averaging over the dominant wave period, and time-averaging over turbulent scales. The decomposed components are assumed to be uncorrelated. By substituting Eq. (1) into the Navier-Stokes equations, the governing

equations of motion in a right-hand Cartesian coordinate system are given as

$$\frac{\partial \bar{u}_i}{\partial x_i} = 0, \tag{2}$$

$$\frac{D\bar{u}_i}{Dt} = -\frac{1}{\rho_a}\frac{\partial \bar{p}}{\partial x_i} - \delta_{i3}g + \nu\frac{\partial \bar{u}_i}{\partial x_i} - \frac{\partial}{\partial x_j}(\overline{u'_j u'_i} + \overline{\tilde{u}_j \tilde{u}_i}), \tag{3}$$

where δ_{i3} is the Kronecker delta function, g is the acceleration due to gravity, ρ_a is the air density, t is time, $-\rho_a\overline{u'_i u'_j}$ and $-\rho_a\overline{\tilde{u}_i\tilde{u}_j}$ are the components of Reynolds and wave-induced stresses, respectively arising from applying decomposition (1), and D/Dt denotes the material derivative. We also denote $x_i = (x, y, z)$ and $u_i = (u, v, w)$, with x directed eastward, y northward, and z upward, where u, v, and w are the corresponding velocity components.

Although Eq. (3) provides modifications of the momentum balance equations above the wavy interface, more assessments of the wave-wind-turbulence interactions are required by investigating the respective turbulent and Wave Kinetic Energy (WKE) equations. Individual components of WKE and the Turbulent Kinetic Energy (TKE) budget, assuming neutrally buoyant flow, a rotational wave field, and neglecting viscous terms are given after Anis and Moum [17] as

$$\frac{1}{2}\frac{\partial \tilde{u}_i^2}{\partial t} = -\overline{\tilde{u}\tilde{w}}\frac{\partial \bar{u}}{\partial z} + \overline{< u'_i u'_j > \frac{\partial \tilde{u}_i}{\partial x_j}} - \frac{\partial}{\partial z}\left[\overline{\tilde{w}\left(\frac{1}{2}\tilde{u}_i^2 + \frac{\tilde{p}}{\rho}\right)} + \overline{< w'u'_i > \tilde{u}_i}\right], \tag{4}$$

$$\frac{1}{2}\frac{\partial u'^2_i}{\partial t} = -\overline{u'w'}\frac{\partial \bar{u}}{\partial z} - \overline{< u'_i u'_j > \frac{\partial \tilde{u}_i}{\partial x_j}} - \frac{\partial}{\partial z}\left[\overline{w'\left(\frac{1}{2}u'^2_i + \frac{p'}{\rho}\right)} + \overline{\left\langle\frac{1}{2}u'^2_i\right\rangle\tilde{w}}\right] - \varepsilon, \tag{5}$$

where $< . >$ denotes the phase averaging, and the first terms on the right-hand side of Eqs. (4) and (5) correspond to the energy transfer from the wave field to the mean flow and mean flow shear production, respectively. The second term describes production of WKE (and TKE) as a result of interaction between the periodic wave shear and Reynolds stresses, the third term represents only transport of the WKE and TKE (neither production nor consumption) and the fourth term on the right-hand side of Eq. (5) represents the viscous dissipation of TKE. Using Eqs. (4) and (5), the vertical wave-modified TKE equation can be simplified as

$$\frac{\partial e}{\partial t} = -\overline{u'w'}\frac{\partial \bar{u}}{\partial z}\overbrace{-\overline{\tilde{u}\tilde{w}}\frac{\partial \bar{u}}{\partial z}}^{1} + \frac{\partial}{\partial z}\left[\frac{1}{\rho}\overline{w'p'} + \overline{e'w'}\right]\overbrace{-\frac{1}{\rho}\frac{\partial \overline{\tilde{w}\tilde{p}}}{\partial z}}^{2} - \varepsilon = 0, \tag{6}$$

where $e = \overline{(u'^2 + w'^2)}/2$ and $e' = (u'^2 + w'^2)/2$ are the TKE and its fluctuation, respectively. Term 1 describes the wave-induced energy flux, and the third term corresponds to the vertical rate of change of energy flux due to the correlation between $\tilde{p}$ and the vertical component of orbital velocity, $\tilde{w}$. Hence, the momentum and energy equations for the mean flow driven by the wave and wind under the assumptions of horizontal homogeneity, no horizontal pressure gradients, and no Coriolis force effects become:

$$\frac{\partial \bar{u}}{\partial t} = -\frac{1}{\rho}\frac{\partial}{\partial z}\left[K_m\frac{\partial \bar{u}}{\partial z} + \tau_{wx}\right], \tag{7}$$

$$\frac{\partial \bar{v}}{\partial t} = -\frac{1}{\rho}\frac{\partial}{\partial z}\left[K_m\frac{\partial \bar{v}}{\partial z} + \tau_{wy}\right], \tag{8}$$

$$\frac{\partial e}{\partial t} = -\frac{1}{\rho}\frac{\partial}{\partial z}\left(K_e\frac{\partial e}{\partial z}\right) + P - \varepsilon, \tag{9}$$

$$\frac{\partial \varepsilon}{\partial t} = -\frac{1}{\rho}\frac{\partial}{\partial z}\left(K_\varepsilon\frac{\partial \varepsilon}{\partial z}\right) + \frac{\varepsilon}{e}(c_{1\varepsilon}P - c_{2\varepsilon}\varepsilon), \tag{10}$$

where the second-order moments in Eqs. (7)–(10) are obtained using the following closure assumption:

$$-\overline{u'w'} = K_m\frac{\partial \bar{u}}{\partial z}; \quad -\overline{v'w'} = K_m\frac{\partial \bar{v}}{\partial z};$$
$$-\overline{e'w'} = K_e\frac{\partial e}{\partial z}; \quad -\overline{\varepsilon'w'} = K_\varepsilon\frac{\partial \varepsilon}{\partial z}; \tag{11}$$

The eddy viscosity for momentum is expressed using the Kolmogorov equation

$$K_m = c_\mu \frac{e^2}{\varepsilon}, \tag{12}$$

where c_μ is a constant, and the eddy viscosities for TKE and ε are parameterized in terms of the turbulent eddy viscosity:

$$K_e = \frac{K_m}{\sigma_e}; \quad K_\varepsilon = \frac{K_m}{\sigma_\varepsilon}; \tag{13}$$

Corresponding values of all model parameters are listed in Table 1. The wave-wind induced production term, P, is

Table 1. The turbulence closure parameters.

Coefficient	c_μ	σ_e	σ_ε	$c_{1\varepsilon}$	$c_{2\varepsilon}$	$c_{3\varepsilon}$	κ
	0.0054	1	1	3.7	1.92	1.3	0.41

specified as:

$$P = K_m \left[\left(\frac{\partial \bar{u}}{\partial z} \right)^2 + \left(\frac{\partial \bar{v}}{\partial z} \right)^2 \right] + \tau_{wx} \frac{\partial \bar{u}}{\partial z} + \tau_{wy} \frac{\partial \bar{v}}{\partial z}, \tag{14}$$

where $\tau_{wx} = -\rho \overline{\tilde{u}\tilde{w}}$ and $\tau_{wy} = -\rho \overline{\tilde{v}\tilde{w}}$ are the horizontal components of wave-induced stress. It should be noted that we neglected the pressure correlation contribution to simplify the problem. The boundary conditions for the momentum equations (7) and (8) for the MABL are given by

$$\left[K_m \frac{\partial \bar{u}}{\partial z} \right]_{z=H} = u_{*a}^H; \quad \left[K_m \frac{\partial \bar{u}}{\partial z} \right]_{z=z_{0s}} = u_{*a}^0; \tag{15}$$

where z_{0s} is the aerodynamic roughness length at the sea surface, H denotes the height of the MABL, and u_{*a}^H and u_{*a}^0 are friction velocities at height H and at the sea surface, respectively. We also set zero flux boundary conditions for the v-component of the wind at both the sea surface and the height H. Furthermore, boundary conditions for TKE and its dissipation are set by:

$$[\varepsilon]_{z=H} = \frac{(u_{*a}^H)^3}{\kappa H}; \quad \left[K_\varepsilon \frac{\partial \varepsilon}{\partial z} \right]_{z=z_{0s}} = \frac{(u_{*a}^0)^4}{h_1 c_{1\varepsilon}}; \quad \left[K_e \frac{\partial e}{\partial z} \right]_{z=H,z_{0s}} = 0; \tag{16}$$

where h_1 is the thickness of the grid cell adjacent to the surface.

3. Wave-induced stress

The action of wind over the ocean injects momentum into both the MABL and OBL by the means of form drag of the sea surface. This drag is defined as a correlation between the sea surface slope and the wave-induced surface pressure. Near the sea surface the form drag satisfies the following relation:

$$\tau_{tot} = \rho_a C_D u_{*a}^2 \simeq \tau_t + \tau_\nu + \tau_w, \tag{17}$$

where ρ_a is the water-side density, C_D is the drag coefficient, τ_ν is the viscous stress at the interface which becomes valid in the viscous layer, and τ_t is the turbulent stress. Hence, the wave-induced momentum stress (form drag) can be calculated by virtue of τ_t and τ_ν. The wave-induced momentum flux can also be determined using wave energy spectrum information:

$$\tau_w = \rho_w g \int \frac{S_{in}(f)}{c_p} \hat{\mathbf{k}} \, df, \tag{18}$$

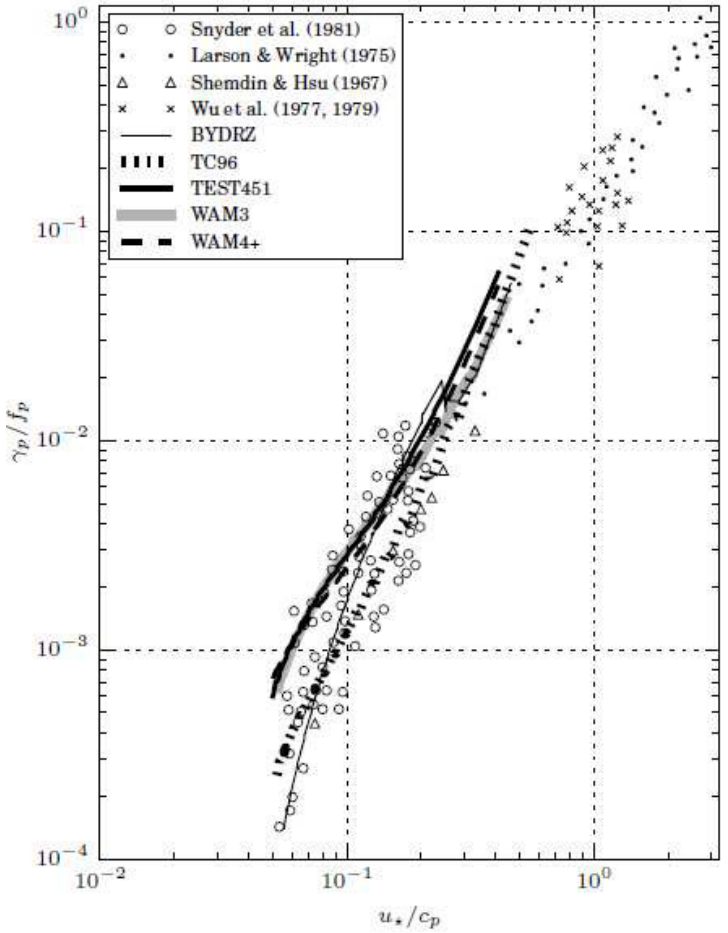

Fig. 1. Dimensionless growth rate corresponding to Snyder et al. [18] (thick gray line), Ardhuin et al. [19] (thick black line). Babanin et al. [20] and Rogers et al. [21] (BYDRZ thin line), and Tolman and Chalikov [23] (TC96) (dotted line). The dashed line represents WAM Cycle 4 with modifications by Janssen [24] and Bidlot et al. [25]. The triangles, circles, dotes, and crosses are from the laboratory and field observations made by Shemdin and Hsu [26], Snyder et al. [18], Larson and Wright [27] and Wu et al. [28,29], respectively. The growth rate estimates have been provided by Tolman [30].

where c_p is the wave phase speed according to the linear dispersion relation, f is frequency in Hz, $\hat{\mathbf{k}}$ is the wave direction, ρ_w is the water-side density, and $S_{in}(f) = \gamma E(f)$ is the energy input from the wind to waves, γ being the growth rate of wind-generated waves [15]. Here, E denotes the non-directional wave energy spectrum. To discuss the physics of wind-wave interaction, we illustrate (Fig. 1) the growth rate of wind-generated waves in which the shape of the wave energy spectrum is given by the Joint North Sea Wave Project (JONSWAP) theoretical spectrum:

$$E(f) = \frac{\alpha g^2}{(2\pi)^4 f^5} \exp\left[-\frac{5}{4}\frac{f}{f_p}\right]^{-4} \gamma_e^{\exp[-1/2[(f-f_p)/(\sigma f_p)]^2]} \tag{19}$$

where $\sigma = 0.07(0.09)$ for $f \leq f_p$ ($f > f_p$), $\gamma_e = 3.3$, $\alpha = 0.0081$, and f_p is the peak frequency of the wave energy spectrum.

The importance of the growth rate parameterization is shown in Fig. 1. Analytical and numerical studies have suggested that the growth rate is proportional to the square of the friction velocity as $\gamma \sim (u_{*a}/c_p)^2\beta$, where β is the growth rate parameter. The friction velocity should be determined from local turbulent stress as difference between total stress and wave-induced stress rather than by using the square root of total stress (Eq. 17). This is because

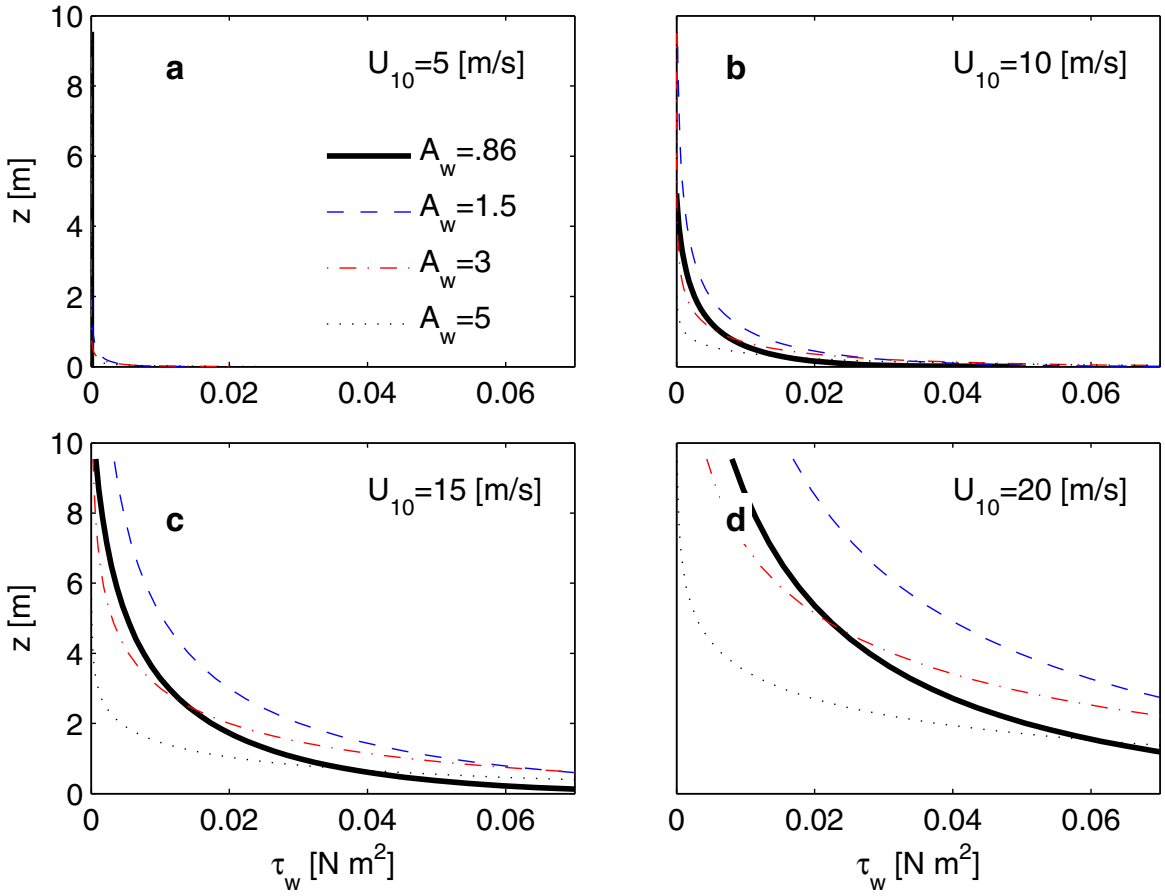

Fig. 2. Vertical distributions of wave-induced stress for different inverse wave ages, A_w, and values of U_{10} at H = 10 m.

close to the sea surface the wave forcing gives rise to a substantial fraction (τ_w) of the total stress amount (τ_{tot}). In Figure 1, the dimensionless growth rate γ/f is shown as a function of u_{*a}/c_p for various wave conditions. Here the growth rates as suggested by Snyder et al. [18], source terms in BYDRZ (Babanin et al. [20] and Rogers et al. [21]), and TC96 are compared with observational data compiled from Plant [22]. Parameterizations suggested by Snyder et al. [18] give the largest growth rate for strongly forced waves with a slight overestimation of Shemdin and Hsu [26] data. BYDRZ and TC96 give the highest correlations with the observed growth rate for weakly forced waves, and also give a better fit with Snyder et al. [18] and Shemdin and Hsu [26] data for strongly forced waves. However, the agreements between growth rate predictions and observations provide strong support for the aforementioned theories and parameterizations of wind generated wave growth rate.

4. Numerical results

The numerical experiments are conducted for various wind speeds and wave ages to study wave-wind-turbulence interactions and to investigate the distribution of momentum flux and turbulent structures in the MABL. Here, we use a steady-state k–ε model with the minimum values assigned for initializing the TKE and its dissipation rate. We use vertical non-equidistance higher resolution with a slight zooming to the surface (with an approximate resolution of 0.2 m).

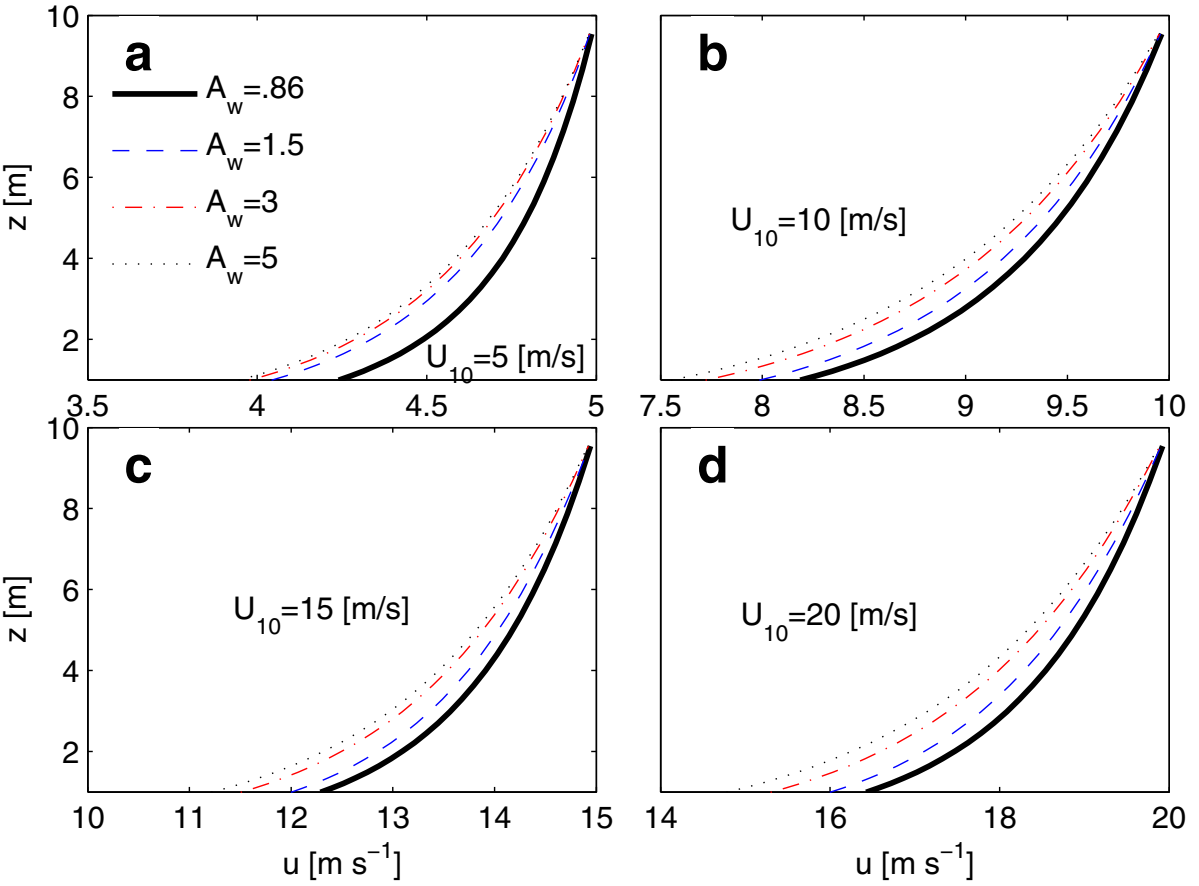

Fig. 3. Wind speed profiles for different inverse wave ages and values of U_{10} at $H = 10$ m.

Surface wave-induced stresses together with wind and wave information for various wind and wave conditions are given in Fig. 2. The wave-induced stress is calculated based on CR11 [15]. In the theory developed in the present study, the wave-induced stress plays a significant role in both transporting momentum and injecting energy into the overlying atmosphere. Thus, we provide a vertical distribution of τ_w for different wave ages ($A_w^{-1} = c_p/U_{10}$, where A_w is the inverse wave age) and wind speeds to better illustrate the effects of different physical mechanisms. Therefore, an important question is how the form drag is distributed as a decaying function of height. To answer, it should be pointed out that this is a controversial topic for both wave-wind and wave-current interactions. However, an educated guess for the wavenumber component k might be $f(z) = \exp(-2kz)$. Here, we use the same vertical distribution as that introduced in CR11.

To illustrate the significance of the wave effects, we calculate the vertical profiles of the x-component of horizontal velocity for the wavy water surface with different wave ages and wind speeds at the height H of the top of the MABL. As has been already mentioned, stratification effects have been neglected in our simulations for the sake of simplicity. For four different wind speeds (ranging between 5 and 20 m s^{-1}) at the top of the simulation domain, $H = 10$ m, four velocity profiles are presented corresponding to various inverse wave ages (0.85, 1.5, 3, and 5, respectively). The mean flow over the wavy surface is shown for both weak and strong wave and wind forcing. In Fig. 3-a, there is a substantial difference between the swell dominated case, $A_w = 0.855$, and wind seas. The distance decreases with increasing wind speed at height H and with a reduction in the wave forcing (Figs. 3-b,c, and d).

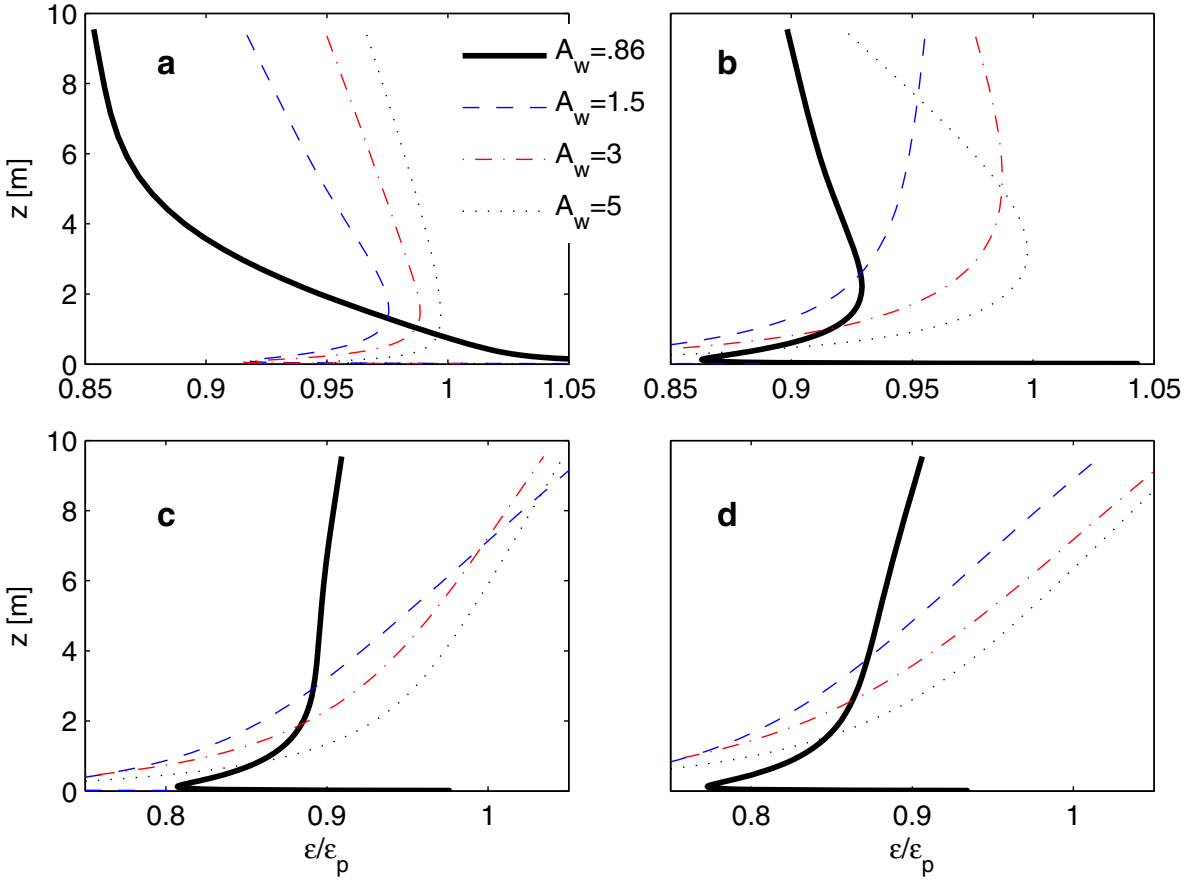

Fig. 4. Vertical distribution of ε for different inverse wave ages and values of U_{10} at H = 10 m.

A number of atmospheric and oceanic measurements have shown that profiles of ε in the MABL are substantially enhanced near the wavy interface. In Fig. 4, we show the vertical distribution of ε in the MABL for similar configurations to the previous test case. In this figure, it can be seen that surface gravity waves strongly influence both the magnitude and vertical distribution of ε near the sea surface. The maximum wave-induced jets occur (in Fig 4-a) at heights around 1 to 1.5 m above the sea surface for $A_w = 0.855$, and increase for the case $U_{10} = 10$ m s^{-1}. The effect of increasing the wind reference value at H is to suppress the wave-induced jet formation when $U_{10} = 15$–20 m s^{-1}.

5. Conclusions

A wave-modified numerical scheme has been developed which calculates the coupling between waves and the atmosphere, based on the method of CR11. The main modification with respect to CR11 was to derive governing equations of motion and energy in a simplified way and to explain the turbulence structure above a wavy rough sea surface. This also gives us the opportunity to further develop this model to take more complex factors into account, in particular, when stratification has a significant role in both momentum transfer and the energy budget. Use of this one-dimensional model is dependent on the wave-induced stress acting on the sea surface and its vertical distribution. We have briefly presented derivations of the wave-induced drag and its vertical distribution pattern. The simplified model, which assumes horizontal homogeneity and neglects Coriolis and buoyancy contributions, was applied for

two test cases to investigate effect of wave forcing on the mean flow and dissipation rates of TKE. The results are preliminary and merit further investigation.

6. Acknowledgements

This work has been funded by the Norwegian Centre for Offshore Wind Energy (NORCOWE) under grant 193861/S60 from the Research Council of Norway (RCN).

References

[1] Bakhoday-Paskyabi M, Fer I. Turbulence structure in the upper ocean: a comparative study of observations and modelling, Ocean Dyn.; 2014; DOI 10.1007/s10236-014-0697-6.
[2] Harris DL. The wave-driven wind. J. Atmos. Sci.; 1966;23:688–693.
[3] Fabrikant AL. Quasilinear theory of wind-wave generation. Izv. Atmos. Ocean. Phys.; 1976;12:524.
[4] Janssen PAEM. Wave-induced stress and the drag of air flow over sea waves. J. Phys. Oceanogr.; 1989;19:745–753.
[5] Miles JW. On the generation of surface waves by shear flows. J. Fluid Mech.; 1957;3:185–204.
[6] Jenkins AD. A simplified quasilinear model for wave generation and air-sea momentum flux. J. Phys. Oceanogr.; 1993;23:2001–2018.
[7] Jenkins AD. A quasi-linear eddy viscosity model for the flux for the flux of energy and momentum to wind waves, using conservation-law equations in a curvilinear coordinate system. J. Phys. Oceanogr.; 1992;22:843–858.
[8] Sullivan PP, McWilliams JC, Moeng CH. Simulation of turbulent flow over idealized water waves. J. Fluid Mech.; 2000;404:47–85.
[9] Kudryavtsev VN, and Makin VK. Impact of swell on the marine atmospheric boundary layer. J. Phys. Oceanogr.; 2004;34:934–949.
[10] Belcher SE, Hunt JCR. Turbulent shear flow over slowly moving waves. J. Fluid Mech.; 1993;251:109–148.
[11] Semedo A, Sætra Ø, Rutgersson A, Kahma KK, Pettersson H. Wave-induced wind in the marine boundary layer. J. Atmos. Sci.; 2009;66:2256–2271.
[12] Yelland M, Taylor PK. Wind stress measurements from the open ocean. J. Phys. Oceanogr.; 1996;26:541–558.
[13] Donelan MA, Drennan WM. Nonstationary analysis of the directional properties of propagating waves. J. Phys. Oceanogr.; 1996;26:1901–1914.
[14] Babanin AV, Makin VK. Effects of wind trend and gustiness on the sea drag: Lake George study, J. Geophys. Res. 2008;113.
[15] Chalikov D, Rainchik S. Coupled numerical modelling of wind and waves and theory of the wave boundary layer, Bound. Layer Meteorol.; 2011;138:1–41.
[16] Ting CH, Babanin AV, Chalikov D, Hsu TW. Dependence of drag coefficient on the directional spreading of ocean waves. J. Geophys. Res.; 2012;117:1–7.
[17] Anis A, Moum JN. Surface wave-turbulence interactions: Scaling $\epsilon(z)$ near the sea surface. J. Phys. Oceanogr.; 1995;25:2025–2045.
[18] Snyder RL, Dobson F, Elliott J, Long RB. Array measurements of atmospheric pressure fluctuations above surface gravity waves. J. Fluid Mech.; 1981;102:1–59.
[19] Ardhuin F, Rogers E, Babanin A, Filipot JF, Magne R, Roland A, van der Westhuysen A, Queffeulou P, Lefevre JM, Aouf L, Collard F. Semi-empirical dissipation source functions for wind-wave models: Part I, definition, calibration and validation. J. Phys. Oceanogr.; 2010;40(9):1917–1941.
[20] Babanin AV, Young IR. Two-phase behaviour of the spectral dissipation of wind waves, Proc. Ocean Waves Measurement and Analysis, Fifth Intern. Symposium WAVES2005, 3–7 July, 2005, Madrid, Spain, Eds. B Edge and JC Santas, Paper No. 51, 11p.
[21] Rogers WE, Babanin AV, Wang DW. Observation-consistent input and whitecapping dissipation in a model for wind-generated surface waves: Description and simple calculations. J. Atmos. Oceanic Technol.; 2012;29:1329–1346.
[22] Plant WJ. A relationship between wind stress and wave slope. J. Geophys. Res.; 1982;87:1961–1967.
[23] Tolman HL, Chalikov D. Source terms in a third-generation wind wave model, J. Phys. Oceanogr.; 1996;26:2497–2518.
[24] Janssen PAEM. The interaction of ocean waves and wind. Cambridge University Press; 2004.
[25] Bidlot JR, Abdalla S, Janssen PAEM. A revised formulation for ocean wave dissipation in CY25R1. Tech. Rep. Memorandum R60.9/JB/0516, Research Department, ECMWF, Reading, UK; 2005.
[26] Shemdin OH, Hsu EY. Direct measurement of aerodynamic pressure above a simple progressive gravity wave. J. Fluid Mech.; 1967;30:403–416.
[27] Larson TR, Wright JW. Wind-generated gravity-capillary waves: laboratory measurements of temporal growth rates. J. Fluid Mech.; 1975;70:417–430.
[28] Wu HY, Hsu EY, Street RL. The energy transfer due to air-input, non-linear wave-wave interactions and white-cap dissipation associated with wind-generated waves. Dept. Civ. Eng. Tech Rep., Stanford Univ., Stanford, Calif.; 1977;No. 207.
[29] Wu HY, Hsu EY, Street RL. Experimental study of non-linear wave-wave interaction and white-cap dissipation of wind-generated waves. Dyn. Atmos. Oceans; 1979;3:55–78.
[30] Tolman HL. The WAVEWATCH Development Group. User manual and system documentation of WAVEWATCH III ® version 4.18. National Centers for Environmental Prediction (MMAB Contribution No. 316); 2014;302p.